Sampled current voltammetry for kinetic studies on materials unsuitable for rotating discs or microelectrodes: application to the oxygen reduction reaction in acidic medium

Cybelle Oliveira Soares[a], Oliver Rodríguez[b], Gaetan Buvat[a,c], Matteo Duca[a,d], Sébastien Garbarino[a,e], Daniel Guay[a], Guy Denuault[b]* and Ana C. Tavares[a]*

[a] Institut National de la Recherche Scientifique – Énergie, Matériaux et Télécommunications, 1650 Boulevard Lionel-Boulet, Varennes, Québec J3X 1S2, Canada

[b] Chemistry, University of Southampton, Highfield, Southampton, SO17 1BJ, U.K

[c] Present address: Institut d'Electronique, de Microélectronique et de Nanotechnologies, IEMN CNRS, Avenue Poincaré, 59652, Villeneuve d'Ascq cedex, France

[d] Present address: Quebec Centre for Advanced Materials, Université de Montréal, C.P. 6128, succursale Centre-ville, Montréal, QC H3C 3J7, Canada

[e] Present address: PRIMA Québec, 505 Boulevard Maisonneuve Ouest, Montréal, QC H3A 3C2, Canada

*Corresponding authors :

Ana C. Tavares, E-mail address: ana.tavares@emt.inrs.ca; Phone: + (514) 2286947.

Guy Denuault, E-mail address: G.Denuault@soton.ac.uk; Phone: + (023) 8059 2154.

Abstract

Herein, sampled current voltammetry (SCV) is exploited to study the kinetics of electrochemical reactions with electrode materials that are unsuitable for rotating disc or microelectrode experiments. The approach described opens up the possibility of assessing the electrocatalytic activity of films produced by high throughput deposition techniques, especially conducting films formed on insulators. This is particularly valuable for testing novel oxygen reduction or oxygen evolution catalysts. SCV is a transient technique, yet for processes affected by mass transport, it produces sigmoidal current-voltage curves, which can be analyzed as conventional steady state voltammograms. Selecting different sampling times affords a range of mass transfer coefficients and this is particularly useful to determine kinetic parameters. The applicability of SCV is first assessed with the fast electron transfer between ferri and ferrocyanide ions and an excellent agreement between the SCV and RDE methods is found. Then, SCV is used to investigate the oxygen reduction reaction (ORR) on a stationary polycrystalline Pt disc, on a polycrystalline Pt foil and on a thin Pt film oriented in the (110) direction. The results are systematically compared with those from a rotated polycrystalline Pt disc. Importantly, the sampled current voltammograms (SCVs) are found to be sufficiently sensitive to reveal differences in electrocatalytic activity between the Pt electrodes and between different sulfate concentrations. The technique is thus well adapted to probing variations in catalytic activity due to surface structure or interactions between solution species and surface sites. For polycrystalline Pt, the ORR kinetic parameters obtained from the Koutecký-Levich (K-L) analysis of the SCVs are in good agreement with those obtained with the RDE. Overall, the sampled current voltammetry approach reported here provides a valuable alternative to steady state voltammetry, and it is particularly suited to assess the electrocatalytic properties of surfaces where epitaxial thin film electrodes are grown on insulating

substrates. The methodology could easily be extended to other substrates such as catalysts deposited on gas diffusion electrodes.

Keywords: Sampled current voltammetry; oxygen reduction reaction; platinum; crystallographic orientation; specific adsorption.

1. Introduction

Sampled current voltammetry (SCV) is a potential step technique where chronoamperograms recorded for a range of target potentials are sampled at a fixed time, and the selected currents plotted against the target potentials to produce a so called sampled current voltammogram (SCV). If only one sampling time is used, the technique is known as normal pulse voltammetry [1, 2]. By sampling the transients over a range of timescales, a whole family of SCVs can be produced, Figure 1, and more information is available. Sampling at a fixed time removes the time dependence of the current intensity and for a soluble reactant undergoing an electron transfer affected by mass transport, the sampled current voltammograms have a sigmoidal shape irrespective of the chosen sampling time [3]. However, the SCV currents scale with the mass transfer coefficient and decrease as the sampling time increases. As with voltammetric waves recorded at rotating disc or microdisc electrodes under steady state conditions, the analysis of SCV waves is simpler than that of conventional voltammograms. In particular, it is possible to compare the shape of SCVs recorded at different times to reveal subtle kinetic effects [3]. For long sampling times the waves are under mass transport control and yield no kinetic information, but for short sampling times the rising part of the waves becomes distorted by electron transfer kinetics. We have exploited this approach to derive kinetic information from SCVs obtained with microdisc Pt electrodes [3]. In common with other electroanalytical techniques, the starting potential is selected from a region where no reaction occurs to an appreciable extent. In absence of irreversible surface processes, the target potentials can be randomly selected within the window of interest. But when the electrode reactions involve adsorbed species it is possible to condition the electrode surface, electrochemically or otherwise, before each potential step to ensure that every chronoamperogram arises from the same initial condition. In this way, all the SCV data points share the same electrode

history; this contrasts with linear and cyclic voltammetry where every data point reflects the evolving state of the electrode surface. We have exploited this approach to investigate the oxygen reduction reaction (ORR) on Pt microelectrodes [4, 5].

Herein we demonstrate that SCV can be used to study the kinetics of electrochemical reactions on macroscopic electrodes which cannot be made into rotating discs or microelectrodes. We start with a stationary Pt disc and validate the SCV results by comparing with those from the same disc under rotation. We then exploit SCV to investigate the ORR on a polycrystalline Pt foil and on a single crystal film of Pt deposited on an insulator. We have selected the ORR as a test case because the most common methodology to study the reaction involves forced convection techniques such as the rotating disc and rotating ring disc electrodes [6, 7]. The performance of a novel ORR electrode material or catalyst is normally compared to that of platinum based electrodes [8-11], but the approach is only viable if the material can be machined as a disc electrode or if the catalyst can be dispersed in a slurry to coat the surface of a rotating disc electrode. In this article, we therefore present SCV as a methodology to study the electrocatalytic properties of complex surfaces where, for example, polycrystalline or epitaxial thin film electrodes are grown on insulating substrates or catalysts are deposited on gas diffusion electrodes. For such materials the traditional RDE and microelectrode [12] methodologies are not suitable.

In the first part of the paper, we derive the conditions where the SCVs obtained by sampling the current transients are analogous to the linear sweep voltammograms recorded with the RDE. In the second part, we illustrate the comparison between SCV and RDE with a model redox process, the electron transfer between the ferri and ferrocyanide ions. In the third part, we continue the comparison with a more complex process, the oxygen reduction reaction on polycrystalline Pt electrodes. In the final part, we exploit SCV to investigate the ORR on a Pt foil and on a (110)

single crystal Pt thin film, the latter being known as the most active facet for the ORR in sulfuric acid electrolyte [13, 14]. We conclude the discussion with an analysis of the strengths and limitations of the technique.

2. Experimental

Materials, electrodes and chemicals: Ultrapure water (Milli-Q, resistivity >18 MΩ cm) was used to prepare all solutions. H_2SO_4 (trace metal grade, Fisher), $K_3[Fe(CN)_6]$ (>99%, Acros Organics), $K_4Fe(CN)_6 \cdot 3H_2O$ (min. 98.5%, Alfa Aesar), KCl (min 99.5%, Bioshop) were used as received. $KClO_4$ (99.99% trace metal grade, Sigma-Aldrich) was re-crystallized in ultrapure water before using. All glassware was soaked in acidic permanganate solution overnight, then immersed in diluted piranha solution and boiled in ultrapure water several times. Experiments were conducted with three electrodes: a polycrystalline Pt RDE (Pine Research, 5 mm Ø), a Pt foil (99.9%, Alfa Aesar) and a Pt single crystal thin film with a (110) orientation (Pt thin film deposited on (110) MgO substrate, hereafter denoted Pt/MgO (110)). Before each experiment, the Pt RDE was polished with alumina slurries with grain sizes of 1, 0.3 and 0.05 μm on a polishing micro-cloth (both from Buehler). Afterwards, the Pt disc was rinsed thoroughly with MilliQ water and sonicated for 10 min. The polycrystalline Pt foil was flamed annealed before each experiment. The Pt/MgO (110) thin film was prepared by pulsed laser deposition and the details are provided in the supplementary information (SI). Structural and electrochemical characterization, Figures S1-3, evidenced that the thin film was oriented in the (110) direction and that its electrochemical behavior was very similar to that of single crystal Pt(110) – (1×2) reconstructed surfaces [15-17].

RDE experiments were carried out in a conventional one compartment electrochemical cell (Pine Research), equipped with a Pt gauze as the counter electrode and a mercury-mercurous sulfate electrode (MMSE - Koslow) as the reference electrode. The RDE was prepared as described above, and then cycled between 0.050 V and 1.40 V *vs*. RHE at 200 mV s^{-1} in N_2 saturated 0.5 M H_2SO_4 until a stable cyclic voltammogram was recorded. Afterwards, it was used either with the 4 mM $K_3Fe(CN)_6$ / $K_4Fe(CN)_6$ in N_2-saturated 1 M KCl, or in N_2/O_2-saturated 0.5 M H_2SO_4. Before each measurement, the electrolyte solution was purged with N_2 (Praxair, 99.999%) or O_2 (Praxair, 99.993%) for at least 45 min. For the ORR studies, background curves were recorded in N_2-saturated electrolyte and subtracted from the total currents recorded in O_2-saturated electrolyte; the same potential waveform was used in each case. Measurements were carried out at room temperature (23±1 ◦C) using an Autolab PSTAT302 potentiostat controlled by NOVA 2.1.2 (Ecochemie). All potentials are reported versus the reversible hydrogen electrode (RHE). The MMSE reference electrode was calibrated in 0.5 M H_2SO_4 against a homemade RHE ($E_{MMSE} = E_{RHE} - 0.703$ V in 0.5 M H_2SO_4).

SCV experiments were conducted in the conventional three electrode cell equipped with the Pt RDE electrode (electron transfer between $[Fe(CN)_6]^{3-}$ and $[Fe(CN)_6]^{4-}$ and ORR) and in an electrochemical cell specifically designed for the film electrodes, Figure S4. Additional information regarding the cell can be found in the SI. Dedicated potential waveforms were used to record the SCVs. In brief, the electrode potential was first cycled between the upper and lower potential limits at 500 mV s^{-1} to condition the electrode; then, the potential was held at the rest potential (near the open circuit potential) for a specific time, stepped to the target potential of interest and finally stepped back to the rest potential. This procedure was repeated for all the potentials of interest, starting at the lower limit and increasing the target potential until the upper

limit was reached. In each case the conditioning CVs and the current transients were recorded. For the $[Fe(CN)_6]^{3-}$ / $[Fe(CN)_6]^{4-}$ redox pair, the rest potential was held for 10 s, stepped to the potential of interest for 5 s and stepped back to the rest potential for 10 s, this waveform is presented in Figure S5(a). Here the experiments were performed with an equimolar concentration of each ion so the rest potential was chosen to ensure the faradaic current was zero while the rest duration was adjusted to make sure the subsequent potential step was unaffected by the pre-conditioning cycles. This was verified by simulating the evolution of the concentration profiles and current response throughout the conditioning cycles, rest and potential step with DigiElch 8.0 (Gamry Instruments) – the simulated data is shown in the Figure S6.

For the ORR, a similar waveform was used [3, 4], Figure S5(b). After the conditioning of the electrode the potential was held at the rest potential for 60 s, stepped to the potential of interest for 1 s and finally stepped to the rest potential for 20 s. The rest potential duration was set long enough to allow the replenishment of O_2 at the electrode surface before stepping to ORR potential. Finally, a different waveform was employed with the Pt(110) thin film electrodes, which were found to be modified during the conditioning cycles, Figure S5(c). For these electrodes, the conditioning cycles were removed and only the potential rests and steps were kept to record the SCVs.

3. Selection of the sampling times

In this section, we exploit the concept of mass transfer coefficient to derive the conditions where the SCVs obtained at a stationary electrode are analogous to the linear sweep

161 voltammograms recorded with the RDE. The limiting current of an electrochemical reaction
162 controlled by mass transport is given by equation (1) [1, 2]:

163 $$i_{lim} = nFAk_m c^b$$ ilim=nFAcb ilim=nFAcb (1)

164 where n, F, and A have their usual meaning, k_m is the mass transfer coefficient and c^b is the bulk
165 concentration of the reactant. This relationship is independent of the technique used to study the
166 reaction, independent of the form of mass transport involved, and is valid for both the RDE and
167 SCV. The mass transfer coefficient is therefore sufficient to establish the correspondence between
168 the sampled current voltammograms and the hydrodynamically controlled linear sweep
169 voltammograms. At the RDE, the steady state mass transfer coefficient is determined by the
170 rotation rate of the electrode, and can be estimated by the following equation [1, 2]:

171 $$k_m = 0.201\ D^{2/3} \nu^{-1/6} \omega^{1/2}$$ (2)

172 where D is the diffusion coefficient (in $cm^2\ s^{-1}$) of the reactant, ν the kinematic viscosity of the
173 electrolyte (in $cm^2\ s^{-1}$), and ω is the rotation rate (in rpm). Since D and ν are usually known, the
174 values of k_m can be easily calculated for each rotation rate. Conversely, for a potential step, the
175 mass transfer coefficient is determined by the sampling time, τ at which the current is read.
176 Assuming the process is controlled by planar diffusion, k_m is given by equation (3) [1]:

177 $$k_m = \sqrt{\frac{D}{\pi\tau}}$$ (3)

178 Therefore, by combining equations (2) and (3) it is possible to estimate the sampling time required
179 to match a sampled current voltammogram recorded at a stationary electrode with a linear sweep
180 voltammogram recorded at the RDE. For the reduction of ferricyanide, Table 1 shows the sampling
181 times calculated for selected rotation rates. Table 2 presents similar calculations for the reduction

of oxygen. In each case, the sampling times required to equal the mass transfer coefficients produced by the RDE are easily achievable with commercially available electrochemical workstations, even for the fastest rotating electrode. However, when working at such short time scales, it is worth considering the impact of non-faradaic processes, such as double layer charging. The time constant, t_{dl} for the charge and discharge of the double layer is given by equation (4) [1, 2]:

$$t_{dl} = R_s C_{dl} \quad (4)$$

where R_S corresponds to the electrolyte resistance and C_{dl} is the double layer capacitance. In a potential step experiment, the charging of the double layer is 95% complete at $3\times t_{dl}$. Thus, to totally eliminate the impact of double layer charging on the amperometric response, the shortest sampling time should be at least $5\times t_{dl}$ [1]. R_s and C_{dl} were obtained from electrochemical impedance spectroscopy (EIS) measurements, and typical time constants obtained in this work are 100 µs for the RDE cell and 264 µs for the cell constructed for the stationary electrodes. These values mean that currents sampled above 500 µs for the RDE cell and 1.32 ms for the stationary electrode cell should be unaffected by double layer charging. Since SCV is a transient technique, it is worth recalling that increasing the electrode surface roughness will increase the magnitude and timescale of any current related to surface processes, such as double layer charging, adsorption / desorption and oxidation / reduction of adsorbates. Hence the shortest sampling times will need to be adjusted to minimize these extraneous contributions.

In the following section, we present the experimental results obtained with the ferri / ferrocyanide redox pair.

Table 1. Sampling times needed to ensure the mass transfer coefficients obtained in sampled current voltammetry at a stationary electrode are similar to those obtained in linear sweep voltammetry at a rotating disc electrode. Here, the reaction chosen is the reduction of ferricyanide (D = 7.26×10^{-6} cm^2 s^{-1} [18]) and the kinematic viscosity of the electrolyte (1 M KCl) is assumed to be 0.009 cm^2 s^{-1}.

Rotation rate / Rpm	**k_m × 10^3 / cm s^{-1}**	**Sampling time / ms**
100	1.65	846
400	3.30	212
900	4.96	94
1600	6.61	53
2500	8.26	34
3600	9.91	24
4900	11.6	17

Table 2. Sampling times needed to ensure the mass transfer coefficients obtained in sampled current voltammetry at a stationary electrode are similar to those obtained in linear sweep voltammetry at a rotating disc electrode. Here the reaction chosen is the reduction of oxygen (D= 1.93×10^{-5} cm^2 s^{-1}) and the kinematic viscosity of the electrolyte (0.5 M H_2SO_4) is assumed to be 0.0095 cm^2 s^{-1} [19].

Rotation Rate / Rpm	$k_m \times 10^3$ / cm s^{-1}	Sampling time / ms
100	3.14	622
400	6.29	156
900	9.43	69
1600	12.6	39
2500	15.7	25
3600	18.9	17
4900	22.0	13

4. Results and Discussion

4.1. Application of the SCV method to a model redox couple

The electron transfer between ferricyanide and ferrocyanide was investigated with the Pt RDE under hydrodynamic control for linear sweep voltammetry, Figure 2(a), and under quiescent conditions for sampled current voltammetry, Figure 2(b). The RDE polarization curves follow the typical sigmoidal shape characteristic of voltammograms recorded under steady state conditions with a plateau corresponding to the limiting currents between 0.580 and 0.380 V for the reduction, and 0.900 and 1.200 V for the oxidation, of the electroactive species in solution. The sampled current voltammograms also have a sigmoidal shape, and they appear identical to the RDE voltammograms. For example, the SCV obtained at 94 ms agrees very well with the LSV recorded at 900 rpm, Figure 2(c), and the SCV recorded at 54 ms agrees equally well with the LSV recorded at 1600 rpm, Figure 2(d). In both cases, the curves overlap over the whole potential window. The

limiting currents obtained with SCV are, within experimental error, similar to those obtained with the RDE. Furthermore, and as expected from the Cottrell equation [1], the SCV limiting currents are proportional to the inverse square root of the sampling time, Figure 2(b) insert. These results demonstrate that for a model redox system, sampled current voltammetry at a stationary electrode produces voltammograms similar to those at the RDE when the sampling times and rotation rates are selected to yield the same mass transfer coefficient. Simulations of expected curves for both the hydrodynamic voltammetry with the RDE and the reconstructed SCVs using the data that emulate the experimental conditions were performed, Figure S6. The simulated data predicted the correspondence between the RDE and the reconstructed SCV curves, therefore corroborating the experimental results obtained. In conclusion, these results validate the approach presented in section 3.

4.2. Application of the SCV method to the oxygen reduction reaction on polycrystalline platinum

In this section, we use the oxygen reduction reaction on a polycrystalline Pt disc to further test the sampled current voltammetry method. Following the approach described above, linear sweep voltammograms were first recorded with a polycrystalline Pt RDE at different rotation rates. This was done purely for comparison and is not a necessary part of the SCV method. Then, using the same electrode under quiescent conditions, chronoamperograms were recorded for a range of target potentials within the ORR potential window. To reconstruct the SCVs, the current transients were then sampled at selected times corresponding to the same mass transfer coefficients as with the RDE (see Table 2). Again, this was done purely for comparison with the RDE and any other

252 sampling time could have been chosen. Voltammograms and sampled current voltammograms are
253 presented in Figure 3.

254 The RDE polarization curves, Figure 3(a), exhibit the characteristic features for the diffusion
255 controlled ORR on polycrystalline Pt in sulfuric acid solutions [20-22] : i) a sigmoidal wave, ii) a
256 well-defined plateau for the diffusion controlled currents at potentials below 0.4 V *vs.* RHE, iii)
257 the diffusion limited current increases linearly with the square root of the rotation rate (inset in
258 Figure 3(a)) as predicted by the Levich equation, [1] and iv) an hysteresis due to the presence of
259 Pt oxides formed on the beginning of the cathodic scan [22-25]. The Pt oxides formed between
260 0.85 and 1.10 V *vs.* RHE hinder the ORR and shift the wave to more negative potentials [26, 27].

261 The reconstructed sampled current voltammograms, Figure 3(b), display sigmoidal waves
262 similar to those recorded for the RDE but with some differences. First, the magnitude of the SCV
263 limiting currents is slightly larger. Second, the current at the foot of the ORR wave increases when
264 the sampling time decreases, whereas the foot of the RDE wave remains unaffected irrespective
265 of the rotation rate. Third, the SCVs show a broad peak around 0.6 V *vs.* RHE, which is more
266 evident at shorter sampling times. Fourth, additional peaks appear circa 0.13 and 0.26 V at very
267 short sampling times. To elucidate the nature of those differences and eliminate contributions not
268 associated with oxygen reduction, identical experiments were carried out in N_2-saturated
269 electrolyte and the resulting chronoamperograms were subtracted from those recorded in O_2-
270 saturated electrolyte. The SCVs obtained in the N_2-saturated electrolyte, Figure S7, show a
271 pronounced reduction peak at 0.797 V when sampling at 622 ms and at 0.748 V *vs.* RHE when
272 sampling at 25 ms. This peak is attributed to the reduction of the chemisorbed oxygen species
273 formed when the Pt electrode was held at the rest potential, 1.00 V *vs*. RHE. Since the reduction
274 of these species is a fast process, the peak is larger at short sampling times because the oxide

coverage is significant while at long sampling times the peak virtually disappears as most of the oxide has been reduced. The additional peaks at circa 0.2 and 0.1 V are consistent with the adsorption of hydrogen on the electrode surface. After subtraction of the background currents, Figure 3(c), the SCV limiting currents are closer to those obtained with the RDE. More importantly, the currents at the foot of the ORR wave overlap with one another as observed on the RDE voltammograms. This suggests that the extra current seen at short sampling times at the foot of the SCV wave comes from the reduction of Pt oxides formed during the rest period. When compared directly, Figure 3(d), the background subtracted SCV agrees very well with the cathodic scan of the RDE voltammogram, but does not match the scan in the anodic direction. The match between the cathodic branch of the RDE voltammogram and the SCV arises from a simple fact: in both cases, adsorbed oxygen species hinder the ORR and shift the onset of the reaction to more negative potentials. Such interference is absent in the anodic branch of the RDE.

Lowering the rest potential should decrease the initial oxide coverage and several values were tested to find the optimum rest potential: 0.950, 0.900, 0.877, 0.800 and 0.750 V *vs*. RHE. However, none prevented the formation of oxides. More importantly, these values are in the foot of the ORR wave and led to the depletion of oxygen during the rest period. In oxygenated acidic media, it is not possible to find a suitable rest potential where the Pt surface is free from oxygen species because the onset of oxygen reduction overlaps with the onset of oxide formation. This is intrinsic to the platinum surface in acidic medium [23, 25, 26].

The ORR kinetic currents were extracted from the series of chronoamperograms obtained at the foot of the ORR wave. For each target potential, the inverse of the current was plotted against the square root of time, Figure 4(a), in a manner analogous to the Koutecký-Levich (K-L) analysis of RDE voltammograms where the inverse of the current is plotted against the inverse square root

298 of the rotation rate. At long times the plot is linear because the current only comes from the
299 diffusion controlled reduction of oxygen. However, at short times the plot is no longer linear
300 because of the extra current due to the reduction of oxygen species adsorbed on the electrode
301 surface. Extrapolation of the linear section to very short times corresponding to infinite rates of
302 mass transport yields the inverse of the kinetic current. Figure 4(b) shows the Tafel plots of the
303 ORR kinetic currents extracted from the K-L plots shown in Figure 4(a) and reveals a good
304 agreement between the data derived from the RDE voltammograms and that from the SCV
305 approach. The difference in slopes, circa 112 mV for the RDE and 90 mV for the stationary
306 electrode, is consistent with the electrode spending more time in the oxide region during the
307 potential step than during the potential sweep [23, 28-31]. Since the linear region in the K-L plot
308 is purely diffusion controlled, subtracting the background currents recorded in N_2-saturated
309 electrolyte makes little difference to the kinetic currents and therefore to the Tafel slope.
310
311 **4.3. Application of the SCV method to the ORR on a polycrystalline Pt foil and a Pt(110)**
312 **film**
313 Having demonstrated that sampled current voltammetry gives similar results to the rotating
314 disc electrode, we now employ the technique to probe the oxygen reduction reaction on two
315 stationary electrodes, a polycrystalline Pt foil and a single crystal film of Pt. These surfaces were
316 selected to assess whether SCV was sensitive enough to highlight electroactivity differences as the
317 ORR kinetics is known to depend on crystallographic orientation, presence of spectator anions
318 [20], pH [32, 33], and even surface reconstruction [15]. The cell shown in Figure S4 was used to
319 perform SCV with the Pt/MgO(110) and polycrystalline Pt electrodes. The SCVs recorded with
320 the polycrystalline Pt foil were then compared with the SCVs recorded with the stationary Pt RDE,

see Figure S8(a). The agreement is very good and the Tafel slopes are within experimental errors, Figure S8(b). This therefore confirms that the different cell configuration did not affect the sampled current voltammetry.

It has been documented in the literature that the sulfate ions hinder the ORR due to the specific adsorption of the anions on the platinum surface [20, 31]. We therefore investigated whether SCV could reflect the change of ORR activity of the platinum electrodes with the sulfate concentration. The sulfuric acid concentration was decreased from 0.5 M to 0.05 M and the SCV experiments were replicated and compared. $KClO_4$ 0.1 M was added to the 0.05 M H_2SO_4 solution to maintain the conductivity of the electrolyte and prevent ohmic distortions of the SCVs.

The background subtracted SCVs obtained with the polycrystalline Pt foil in O_2 saturated 0.5 M H_2SO_4 and 0.05 M H_2SO_4 + 0.1 M $KClO_4$, Figure 5(a), clearly show that the higher sulfate concentration inhibits the ORR. In the diluted sulfuric acid solution, the wave shifts by circa 40 mV towards more positive potentials and the ORR starts at more positive potentials. The Tafel plots, Figure 5(b), show higher ORR currents and a smaller slope in the diluted electrolyte, reflecting the better performance of the platinum. This is consistent with the specific adsorption of sulfate anions on Pt which is known to hinder the ORR [20, 31], and it demonstrates that SCV is sufficiently sensitive to reveal the poisoning of the electrode surface.

Finally, the Pt/MgO (110) thin film was used as electrode and its SCV response for the ORR was compared to that of the polycrystalline Pt in O_2 saturated 0.05 M H_2SO_4 + 0.1 M $KClO_4$, Figure 6(a). The SCV curve obtained for the oriented thin film has the expected sigmoidal shape. Its half-wave potential is circa 42 mV more positive than that for the polycrystalline Pt foil. The higher activity of the thin film is also highlighted by the Tafel plots that show a lower slope and higher current densities for the Pt/MgO(110) thin film, Figure 6(b). The results obtained are in

344 good agreement with the literature as the Pt(110) surface is known to be the most active platinum
345 low index crystallographic plane in sulfuric acid solutions [14, 34].

346 When comparing the SCVs obtained for poly-Pt and Pt/MgO(110) thin film, a wave with a
347 maximum at circa 0.70 V *vs* RHE is seen in the thin film polarization curve. This excess charge
348 lies in the potential window where the reduction of the platinum oxide takes place. With poly-Pt,
349 subtraction of the background currents removes almost all of the contribution from the platinum
350 oxide reduction to the ORR currents, and the plateau for the diffusion controlled current is clearly
351 seen. Since all plots presented herein had the background currents subtracted, the SCV data suggest
352 that the excess charge observed in Figure 6(a) comes from an additional coverage of adsorbed
353 oxygen due to the presence of oxygen. The impact of the increased oxide coverage is more
354 noticeable at the shorter sampling times and it is attenuated as the sampling time increases, Figure
355 S9. A similar effect is observed with the Pt RDE, Figure 3(c), and it becomes more apparent at
356 lower sulfate concentration, Figure 5(a). However, the effect seems to be more evident with the
357 oriented thin film.

358 It should be mentioned that the thin film SCVs were recorded with a potential waveform
359 only consisting of rests and steps, Figure S5(c). The conditioning cycles were removed as they
360 were found to change the electrocatalytic activity response from that of Pt(110) to that of poly-Pt.
361 This presumably arises from the introduction of surface defects related to surface oxidation upon
362 cycling, Figure S10. Additionally, the number of transients recorded were also decreased in order
363 to minimize the introduction of the defects in the thin film. Still, the modified waveform was found
364 to produce identical SCVs with the Pt foil. Here we must stress that the need and features of the
365 conditioning waveform will depend on the reaction and electrode material and in this respect, SCV
366 is no different to other electroanalytical techniques.

4.4 Analysis of the strengths and limitations of SCV

Strengths: One of the key advantages of the technique is that when mass transport affects the rate of reaction, SCV produces sigmoidal current-potential curves irrespective of time scale and thus of mass transport regime. It is therefore possible to exploit the analytical procedures developed to study steady state voltammograms and this greatly facilitates the analysis and comparisons of the SCVs. This is what makes SCV so interesting for electrode surfaces not amenable to RDE or microelectrode experiments. With a simple cell design, Figure S4, it is possible to perform SCV with foils and thin films. The approach is particularly suited to epitaxial films deposited on insulators. Performing steady state voltammetry with these kinds of electrode would either require another form of hydrodynamic control (e.g. channel flow cell, wall jet or wall pipe [35-38] or covering the electrode surface with a thin insulating microhole template to form an array of recessed microelectrodes [39]. While the former requires a cumbersome flow control system, a large volume of electrolyte and specific cell configurations, the latter would require templates with different hole diameters to produce a range of mass transfer coefficients with the electrode-cell unit needing reassembling for each mass transfer coefficient. Scanning electrochemical probe techniques, e.g. SECCM, can also be used to assess the electrocatalytic activity of electrode surfaces unsuitable to RDE or microelectrode experiments. While they provide remarkable spatial resolution capable of revealing differences in electrocatalytic activity between grains, step edges, and crystal orientations, [C.-H. Chen, L. Jacobse, K. McKelvey, S. C. S. Lai, M. T. M. Koper and P. R. Unwin, Voltammetric Scanning Electrochemical Cell Microscopy: Dynamic Imaging of Hydrazine Electro-oxidation on Platinum Electrodes, Anal. Chem., 2015, 87, 5782-5789. C. L. Bentley, M. Kang and P. R. Unwin, Nanoscale Surface

Structure–Activity in Electrochemistry and Electrocatalysis, J. Am. Chem. Soc., 2019, 141, 2179-2193.E. Daviddi, K. L. Gonos, A. W. Colburn, C. L. Bentley and P. R. Unwin, Scanning Electrochemical Cell Microscopy (SECCM) Chronopotentiometry: Development and Applications in Electroanalysis and Electrocatalysis, Anal. Chem., 2019, 91, 9229-9237.] they require specific and expensive instrumentation, must be operated by highly trained experimentalists and have remained the expertise of a handful of research groups worldwide.

Hence from an experimental point of view, the SCV method is very easy to perform, even with electrode surfaces not amenable to RDE or microelectrode designs. It does not require dedicated hardware or software, is easily implemented with any conventional electrochemical workstations and can be operated with minimal training.

A second major advantage is that selecting the sampling time affords any number of mass transfer coefficients within a huge range of values. As shown in Table 1 and 2, sampling between 1 s and 20 ms affords k_m values similar to those obtained with a RDE. While sampling below 20 ms affords much larger k_m values comparable to those obtained with small microdisc electrodes. For example sampling at 20 ms generates the same k_m as a 14 µm diameter disc while sampling at 1 ms is equivalent to using a 3 µm diameter disc. Another advantage is that the method allows a conditioning procedure before the step to the target potential. This ensures that every transient is recorded under the same conditions. Thus every point on the SCV is recorded with the same electrode history. This is in contrast with conventional voltammetry where every point on the voltammogram is affected by the previous electrode potential. Although the work presented here exclusively considered an electrochemical conditioning approach, the technique allows other conditioning protocols, e.g. via chemical or photochemical conditioning.

412 *Limitations*: The main drawback of SCV is that it is a transient technique and although the
413 SCVs have sigmoidal shapes akin to steady state voltammograms, they still hold time dependent
414 information. Hence, in common with all transient techniques, the SCV currents are susceptible to
415 distortion by surface processes (e.g. double layer charging and electrochemical activity of
416 adsorbed species) and by instrument limitations (e.g. response time of current amplifier). It is
417 therefore important to select appropriate acquisition conditions (see reference [3] for a discussion
418 of these issues) and in particular adjust the sampling time to account for any changes in the time
419 constant of the surface processes. For example, increasing the electrode surface roughness
420 increases the time constant of all surface processes and the SCV sampling time must be increased
421 accordingly. While the distortion of SCV currents arising from the electrochemical activity of
422 adsorbed species is not an issue at long sampling times, it does limit the shortest sampling times.
423 Here we addressed this issue by recording a background SCV and subsequently subtracting it from
424 the main SCV.
425 Another limitation of the technique is that there is no information arising from the potential
426 direction on the SCVs, in contrast with conventional voltammograms. It is not possible to
427 distinguish a forward or backward SCV since the target potentials can be selected in any order.
428 Finally, SCV cannot afford spatial resolution, unlike scanning electrochemical probe
429 techniques, and only provides a response averaged over the electrode surface.
430

431 **5. Conclusions**

432 This study has demonstrated that sampled current voltammetry is a valuable alternative to
433 steady state voltammetry in cases where the electrode material is not appropriate for RDE or

434 microelectrode experiments. In SCV, sampling times can be easily selected to obtain a range of
435 mass transfer coefficients however, in common with other transient electrochemical techniques,
436 the shortest sampling times available are limited by the double layer charging process and by any
437 surface faradaic process such as oxide formation / reduction or hydrogen adsorption / desorption.
438 The methodology was validated with two reactions, the fast electron transfer between ferri and
439 ferrocyanide ions and the ORR on poly-Pt. In both cases, SCV produced analogous results to the
440 RDE after selecting the sampling times to match the mass transfer coefficients of the RDE. The
441 approach was further demonstrated with the ORR on a polycrystalline Pt foil and on a
442 Pt/MgO(110) thin film electrode, neither of which can be assembled into rotating discs or
443 microelectrodes. The technique was found to be sufficiently sensitive to reveal differences in ORR
444 catalytic activity between the different Pt surfaces. The study also demonstrated that SCVs were
445 sensitive enough to show small changes in ORR catalytic activity arising from different
446 concentrations of supporting electrolyte, specific adsorption of ions and crystallographic
447 orientation. Additionally, the chronoamperometric dataset was easily treated to produce plots
448 analogous to the Koutecký-Levich plots at RDEs, providing further kinetic information on the
449 reaction.

450 In common with other transient techniques SCV has limitations when one tries to operate at
451 short time scales but its ability to afford a huge range of mass transfer coefficients and to produce
452 sigmoidal current-potential curves with a simple electrochemical workstation, simple cell design
453 and without additional hardware, are significant advantages which, in our opinion, outweigh its
454 limitations. More importantly, sampled current voltammetry makes it possible to investigate
455 reactions on electrode materials that do not lend themselves to steady state voltammetry with
456 rotating discs or microelectrodes.

Acknowledgements

This work was supported by the Natural Sciences and Engineering Research Council of Canada (NSERC, Strategic Partnership program). Cybelle Oliveira Soares acknowledges the FRQNT funding by means of the PBEEE merit scholarship and she would also like to acknowledge funding for an internship received from the Engineered Nickel Catalysts for Electrochemical Clean Energy project administered from Queen's University and supported by Grant No RGPNM 477963-2015 under the Natural Sciences and Engineering Research Council of Canada (NSERC) Discovery Frontiers Program. Oliver Rodríguez thanks CONACYT-I2T2 for the scholarship (No. 411294) provided to pursue a PhD in Chemistry at the University of Southampton.

References

[1] A.J. Bard, L.R. Faulkner, N. York, C. bullet, W. Brisbane, S.E. Toronto, ELECTROCHEMICAL METHODS Fundamentals and Applications, 2nd ed., John Wiley & Sons, New York, 2001.

[2] Handbook of Electrochemistry, 1st ed., Elsevier, Amsterdam, 2007.

[3] S.C. Perry, L.M. Al Shandoudi, G. Denuault, Sampled-Current Voltammetry at Microdisk Electrodes: Kinetic Information from Pseudo Steady State Voltammograms, Analytical Chemistry, 86 (2014) 9917-9923.

[4] S.C. Perry, G. Denuault, Transient study of the oxygen reduction reaction on reduced Pt and Pt alloys microelectrodes: evidence for the reduction of pre-adsorbed oxygen species linked to dissolved oxygen, Phys. Chem. Chem. Phys., 17 (2015) 30005-30012.

[5] S.C. Perry, G. Denuault, The oxygen reduction reaction (ORR) on reduced metals: evidence for a unique relationship between the coverage of adsorbed oxygen species and adsorption energy, Phys. Chem. Chem. Phys., 18 (2016) 10218-10223.

[6] N. Ramaswamy, S. Mukerjee, Fundamental Mechanistic Understanding of Electrocatalysis of Oxygen Reduction on Pt and Non-Pt Surfaces: Acid versus Alkaline Media, Advances in Physical Chemistry, 2012 (2012) 1-17.

[7] D.B. Sepa, M.V. Vojnovic, A. Damjanovic, Kinetics and mechanism of O2 reduction at Pt in alkaline solutions, Electrochimica Acta, 25 (1980) 1491-1496.

[8] N.M. Markovic, T.J. Schmidt, V. Stamenkovic, P.N. Ross, Oxygen Reduction Reaction on Pt and Pt Bimetallic Surfaces: A Selective Review, Fuel Cells, 1 (2001) 105-116.

[9] H. Lv, D. Li, D. Strmcnik, A.P. Paulikas, N.M. Markovic, V.R. Stamenkovic, Recent advances in the design of tailored nanomaterials for efficient oxygen reduction reaction, Nano Energy, 29 (2016) 149-165.

[10] M. Shao, Q. Chang, J.-P. Dodelet, R. Chenitz, Recent Advances in Electrocatalysts for Oxygen Reduction Reaction, Chemical Reviews, 116 (2016) 3594-3657.

[11] J. Greeley, I.E.L. Stephens, A.S. Bondarenko, T.P. Johansson, H.A. Hansen, T.F. Jaramillo, J. Rossmeisl, I. Chorkendorff, J.K. Nørskov, Alloys of platinum and early transition metals as oxygen reduction electrocatalysts, Nature Chemistry, 1 (2009) 552-556.

[12] J. Kim, A.J. Bard, Application of the Koutecký-Levich Method to the Analysis of Steady State Voltammograms with Ultramicroelectrodes, Analytical Chemistry, 88 (2016) 1742-1747.

[13] N.M. Markovic, R.R. Adzic, B.D. Cahan, E.B. Yeager, Structural effects in electrocatalysis: oxygen reduction on platinum low index single-crystal surfaces in perchloric acid solutions, Journal of Electroanalytical Chemistry, 377 (1994) 249-259.

[14] N.M. Markovic, H.A. Gasteiger, P.N. Ross, Oxygen Reduction on Platinum Low-Index Single-Crystal Surfaces in Sulfuric Acid Solution: Rotating Ring-Pt(hkl) Disk Studies, The Journal of Physical Chemistry, 99 (1995) 3411-3415.

[15] G.A. Attard, A. Brew, Cyclic voltammetry and oxygen reduction activity of the Pt{1 1 0}-(1 × 1) surface, Journal of Electroanalytical Chemistry, 747 (2015) 123-129.

[16] N.M. Marković, B.N. Grgur, C.A. Lucas, P.N. Ross, Surface electrochemistry of CO on Pt(110)-(1 × 2) and Pt(110)-(1 × 1) surfaces, Surface Science, 384 (1997).

[17] G.A. Attard, K. Hunter, E. Wright, J. Sharman, R. Martínez-Hincapié, J.M. Feliu, The voltammetry of surfaces vicinal to Pt{110}: Structural complexity simplified by CO cooling, Journal of Electroanalytical Chemistry, 793 (2017) 137-146.

515 [18] S.J. Konopka, B. McDuffie, Diffusion coefficients of ferri- and ferrocyanide ions in aqueous
516 media, using twin-electrode thin-layer electrochemistry, Analytical Chemistry, 42 (1970) 1741-
517 1741.
518 [19] M.S. El-Deab, T. Ohsaka, Hydrodynamic voltammetric studies of the oxygen reduction at
519 gold nanoparticles-electrodeposited gold electrodes, Electrochimica Acta, 47 (2002) 4255-4261.
520 [20] I. Katsounaros, W.B. Schneider, J.C. Meier, U. Benedikt, P.U. Biedermann, A. Cuesta, A.A.
521 Auer, K.J.J. Mayrhofer, The impact of spectator species on the interaction of H2O2 with platinum
522 - implications for the oxygen reduction reaction pathways, Physical chemistry chemical physics :
523 PCCP, 15 (2013) 8058-8068.
524 [21] V. Stamenković, T.J. Schmidt, P.N. Ross, N.M. Marković, Surface composition effects in
525 electrocatalysis: Kinetics of oxygen reduction on well-defined Pt3Ni and Pt3Co alloy surfaces,
526 Journal of Physical Chemistry B, 106 (2002) 11970-11979.
527 [22] H.A. Gasteiger, S.S. Kocha, B. Sompalli, F.T. Wagner, Activity benchmarks and
528 requirements for Pt, Pt-alloy, and non-Pt oxygen reduction catalysts for PEMFCs, 2005, pp. 9-35.
529 [23] I.A. Pasti, N.M. Gavrilov, S.V. Mentus, Potentiodynamic Investigation of Oxygen Reduction
530 Reaction on Polycrystalline Platinum Surface in Acidic Solutions: the Effect of the Polarization
531 Rate on the Kinetic Parameters, Int. J. Electrochem. Sci, 7 (2012) 11076-11090.
532 [24] N.M. Marković, P.N. Ross Jr, Surface science studies of model fuel cell electrocatalysts,
533 Surface Science Reports, 45 (2002) 117-229.
534 [25] G. Jerkiewicz, G. Vatankhah, J. Lessard, M.P. Soriaga, Y.-S. Park, Surface-oxide growth at
535 platinum electrodes in aqueous H2SO4 Reexamination of its mechanism through combined cyclic-
536 voltammetry, electrochemical quartz-crystal nanobalance, and Auger electron spectroscopy
537 measurements, Electrochimica Acta, 49 (2004) 1451-1459.

538 [26] E.J. Coleman, A.C. Co, The Complex Inhibiting Role of Surface Oxide in the Oxygen
539 Reduction Reaction, ACS Catalysis, 5 (2015) 7299-7311.
540 [27] Y.-J. Deng, M. Arenz, G.K.H. Wiberg, Equilibrium coverage of OH ad in correlation with
541 platinum catalyzed fuel cell reactions in $HClO_4$, Electrochemistry Communications, 53 (2015) 41-
542 44.
543 [28] D.B. Sepa, M.V. Vojnovic, A. Damjanovic, Reaction intermediates as a controlling factor in
544 the kinetics and mechanism of oxygen reduction at platinum electrodes, Electrochimica Acta, 26
545 (1981) 781-793.
546 [29] A. Damjanovic, V. Brusic, Electrode kinetics of oxygen reduction on oxide-free platinum
547 electrodes, Electrochimica Acta, 12 (1967) 615-628.
548 [30] D.W. Banham, J.N. Soderberg, V.I. Birss, Pt/Carbon Catalyst Layer Microstructural Effects
549 on Measured and Predicted Tafel Slopes for the Oxygen Reduction Reaction, The Journal of
550 Physical Chemistry C, 113 (2009) 10103-10111.
551 [31] J.X. Wang, N.M. Markovic, R.R. Adzic, Kinetic Analysis of Oxygen Reduction on Pt(111)
552 in Acid Solutions: Intrinsic Kinetic Parameters and Anion Adsorption Effects, Journal of Physical
553 Chemistry B, 108 (2004) 4127-4133.
554 [32] M.F. Li, L.W. Liao, D.F. Yuan, D. Mei, Y.-X. Chen, pH effect on oxygen reduction reaction
555 at Pt(111) electrode, Electrochimica Acta, 110 (2013) 780-789.
556 [33] S. Strbac, The effect of pH on oxygen and hydrogen peroxide reduction on polycrystalline Pt
557 electrode, Electrochimica Acta, 56 (2011) 1597-1604.
558 [34] B.N. Grgur, N.M. Marković, P.N. Ross, Temperature-dependent oxygen electrochemistry on
559 platinum low-index single crystal surfaces in acid solutions, Canadian Journal of Chemistry, 75
560 (1997) 1465-1471.

561 [35] R.G. Compton, P.R. Unwin, Channel and tubular electrodes, Journal of Electroanalytical
562 Chemistry and Interfacial Electrochemistry, 205 (1986) 1-20.
563 [36] M.E. Snowden, P.H. King, J.A. Covington, J.V. Macpherson, P.R. Unwin, Fabrication of
564 Versatile Channel Flow Cells for Quantitative Electroanalysis Using Prototyping, Analytical
565 Chemistry, 82 (2010) 3124-3131.
566 [37] A.K. Schuppert, A.A. Topalov, I. Katsounaros, S.O. Klemm, K.J.J. Mayrhofer, A Scanning
567 Flow Cell System for Fully Automated Screening of Electrocatalyst Materials, Journal of The
568 Electrochemical Society, 159 (2012) F670-F675.
569 [38] J.V. Macpherson, Recent Advances in Hydrodynamic Modulation Voltammetry,
570 Electroanalysis, 12 (2000) 1001-1011.
571 [39] J. Guo, E. Lindner, Cyclic Voltammograms at Coplanar and Shallow Recessed Microdisk
572 Electrode Arrays: Guidelines for Design and Experiment, Analytical Chemistry, 81 (2009) 130-
573 138.
574
575

576 **Captions to Figures**

577

578 **Figure 1.** Graphical representation of sampled current voltammetry showing how the current
579 varies with the time and the target potential applied to the electrode. The red lines show the current
580 transients and the green dots illustrate the SCVs reconstructed for selected sampling times.

581

582 **Figure 2.** (a) Voltammograms recorded at 20 mV s^{-1} with a 5 mm Ø Pt RDE in a N_2 saturated 4
583 mM $K_3Fe(CN)_6$ + 4 mM $K_4Fe(CN)_6$ +1 M KCl solution with rotation rates between 100 and 2500
584 rpm. (b) Reconstructed sampled current voltammograms obtained in the same solution using the
585 sampling times from Table 1. Each chronoamperogram was recorded using the potential waveform
586 presented in Figure S5(a). The insets present the limiting currents measured at 0.5 V vs. RHE
587 plotted versus (a) the square root of the rotation rate, and (b) versus the inverse of the square root
588 of the sampling time. (c) Comparison of the LSV recorded at 900 rpm with the SCV taken at 94
589 ms, and (d) at 1600 rpm with the SCV taken at 54 ms. The initial potential for the scans was 0.791
590 V and the potential was scanned in the anodic direction up to 1.18 V vs RHE and then reversed.
591 The potential increments for the SCVs is 10 mV starting from the most negative potential limit
592 (≈0.415 V).

593

594 **Figure 3.** (a) Voltammograms recorded at 20 mV s^{-1} with a 5 mm Ø Pt RDE in O_2 saturated 0.5
595 M H_2SO_4 with rotation rates between 100 and 2500 rpm. The inset shows the dependence of the
596 limiting current measured at 0.350 V vs. the square root of the rotation rate. (b) Sampled current
597 voltammograms obtained in the same solution and same electrode but without rotation. The

598 sampling times came from Table 2. (c) Same SCVs as in (b) but after subtracting the background
599 currents recorded in N_2-saturated 0.5 M H_2SO_4. The inset shows the variation of the limiting
600 current measured at 0.350 V vs. the inverse square root of the sampling time used to reconstruct
601 the SCVs. (d) Comparison between the RDE voltammogram recorded at 1600 rpm and the SCV
602 obtained when sampling at 39 ms. In (a), (b) and (c), the dotted lines indicate the corresponding
603 limiting currents expected with the RDE based on the Levich equation.
604
605 **Figure 4.** (a) Koutecký-Levich analysis of the SCVs shown in Figure 3(b). The dotted lines
606 correspond to linear regressions for the times where the current is purely diffusion controlled. (b)
607 Tafel plot for the ORR kinetic currents, taken from the RDE cathodic sweep from Figure 3(a),
608 (grey circles), and from chronoamperograms without (black squares) and with background
609 subtraction (red squares).
610
611 **Figure 5.** (a) Sampled current voltammograms recorded at 39 ms in O_2 saturated 0.5 M H_2SO_4
612 (black squares) and O_2 saturated 0.05 M H_2SO_4 + 0.1 M $KClO_4$ (red circles) with the Pt foil. (b)
613 Tafel plots for kinetic currents taken from Koutecký-Levich plots of the data shown in (a).
614
615 **Figure 6.** (a) Background subtracted sampled current voltammograms recorded in O_2 saturated
616 0.05 M H_2SO_4 + 0.1 M $KClO_4$ for the Pt foil and the Pt/MgO(110) thin film sampled at 39 ms. (b)
617 Tafel plots for kinetic currents taken from Koutecký-Levich plots of the data shown in (a).
618

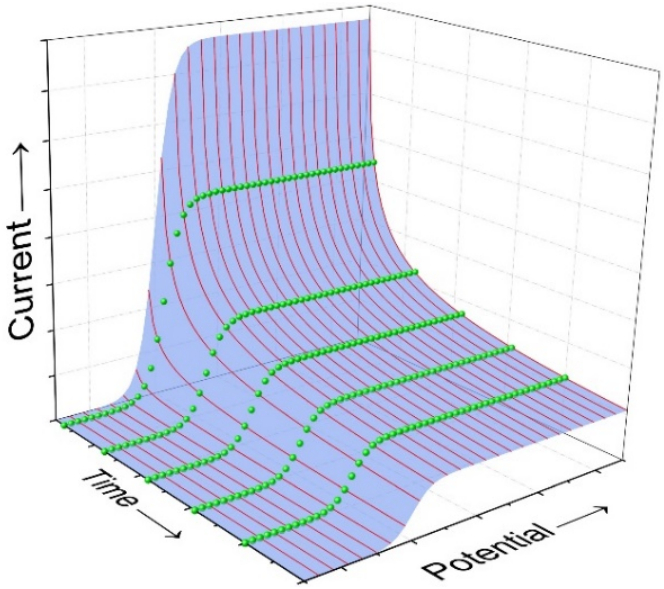

619

620 **Figure 1**

621

622

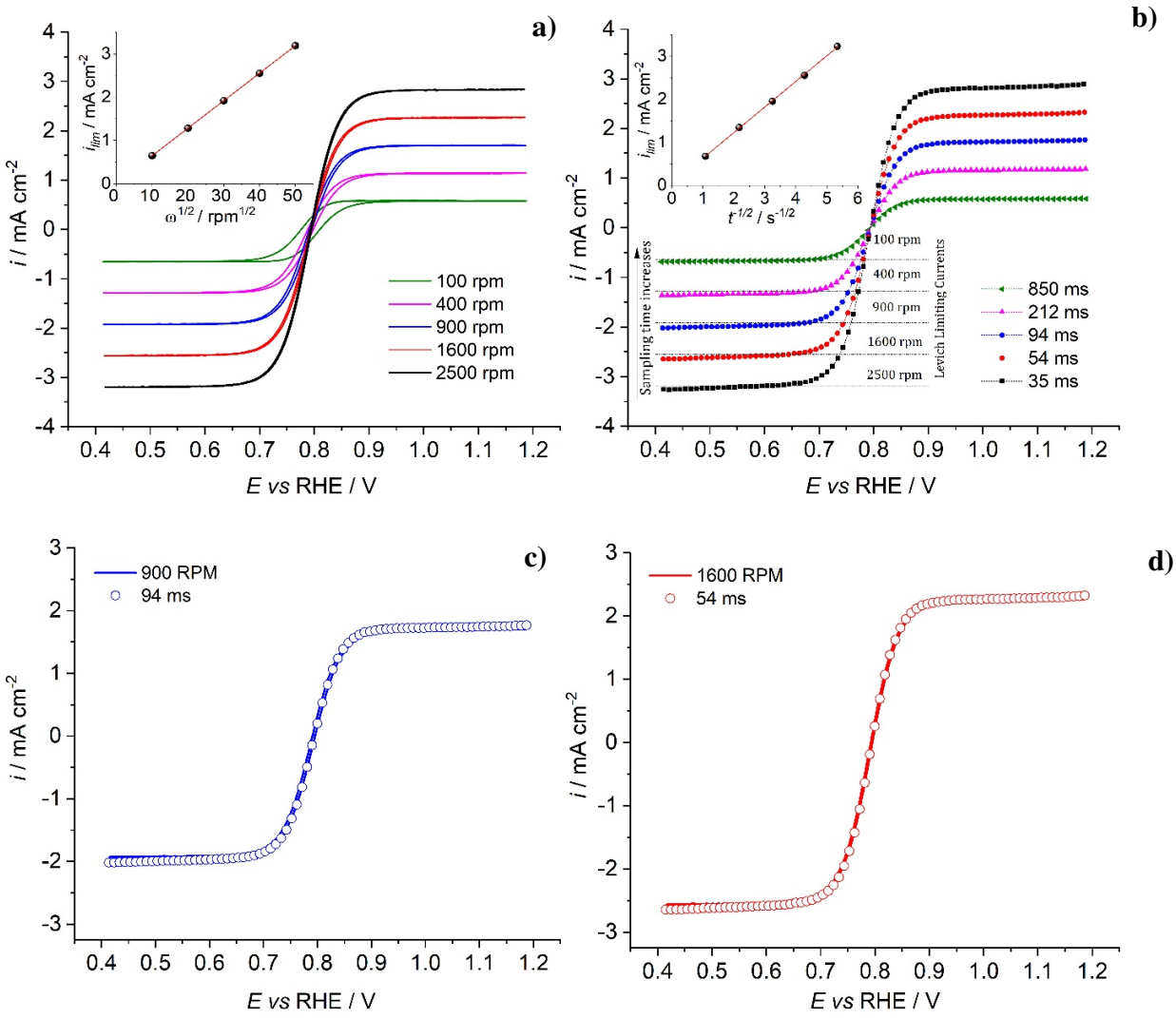

623

624

625 **Figure 2**

626

627

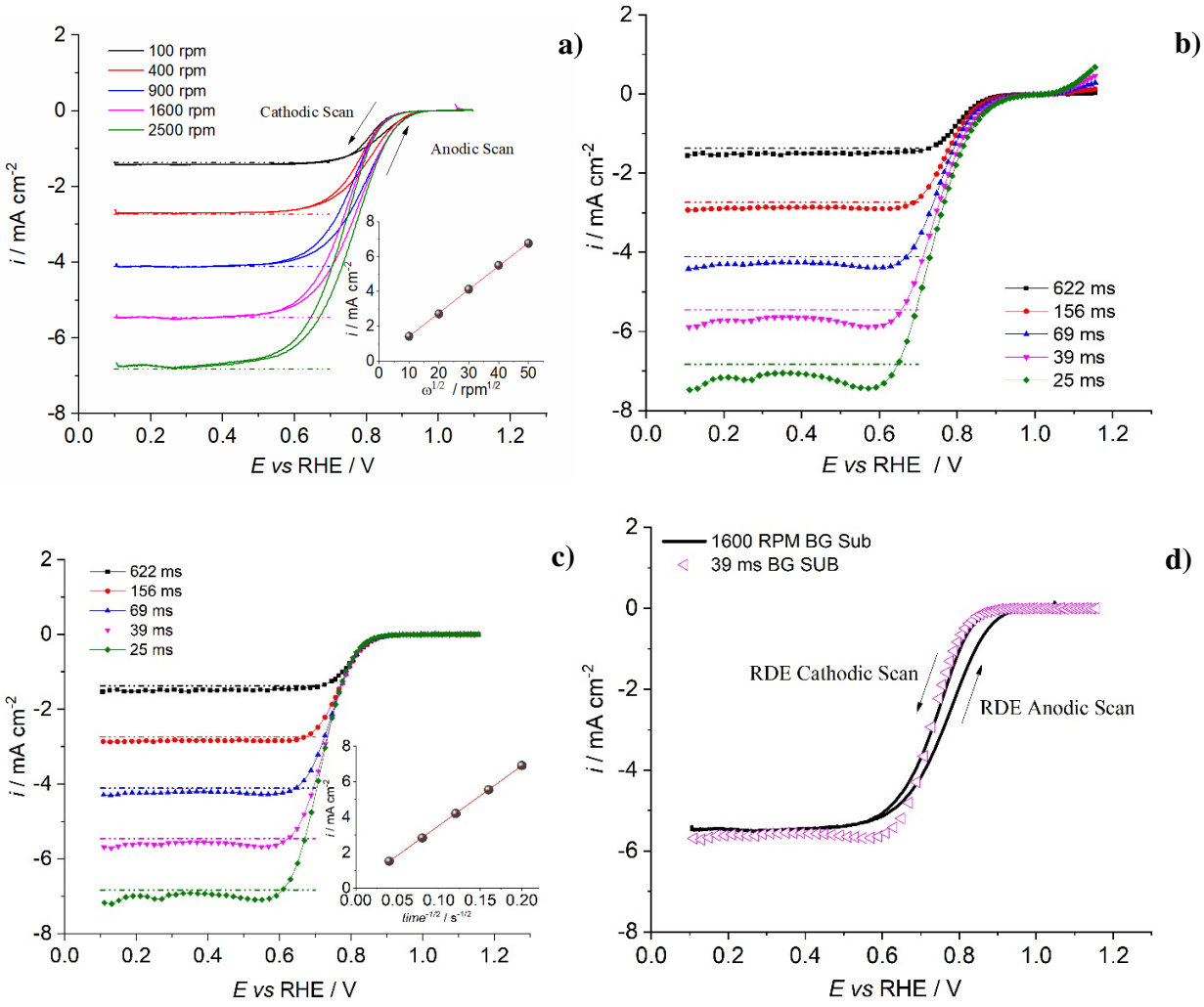

628

629 **Figure 3**

630

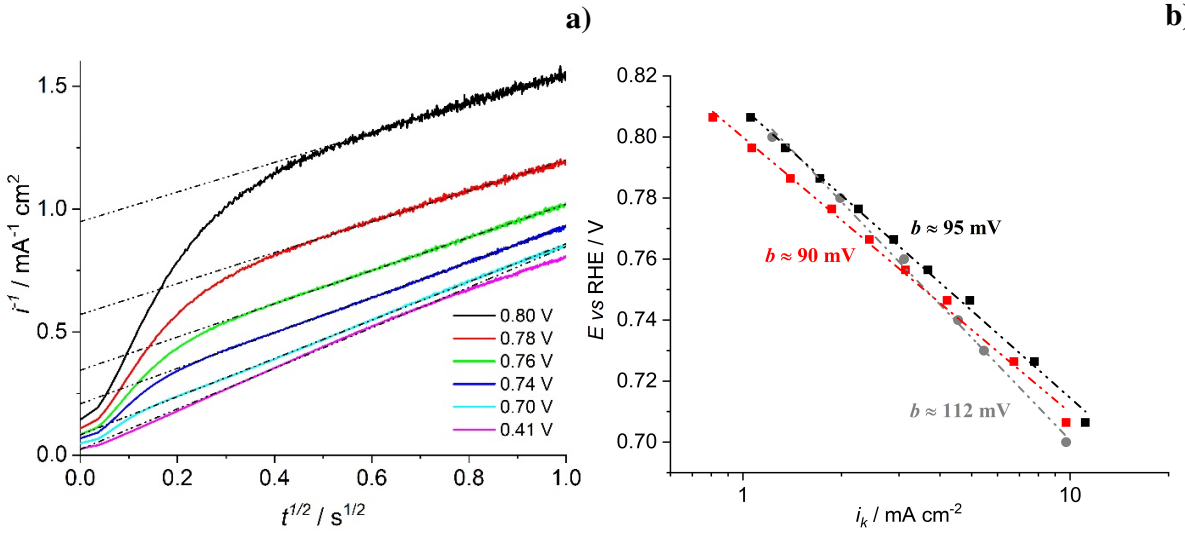

631

632 **Figure 4**

633

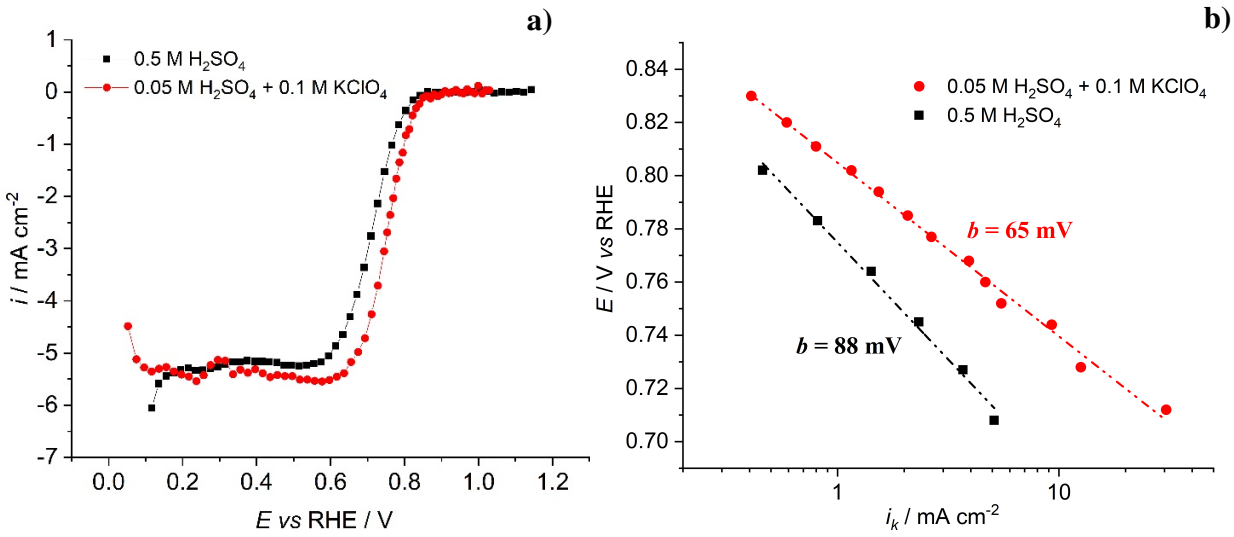

634

635 **Figure 5**

636

a) b)

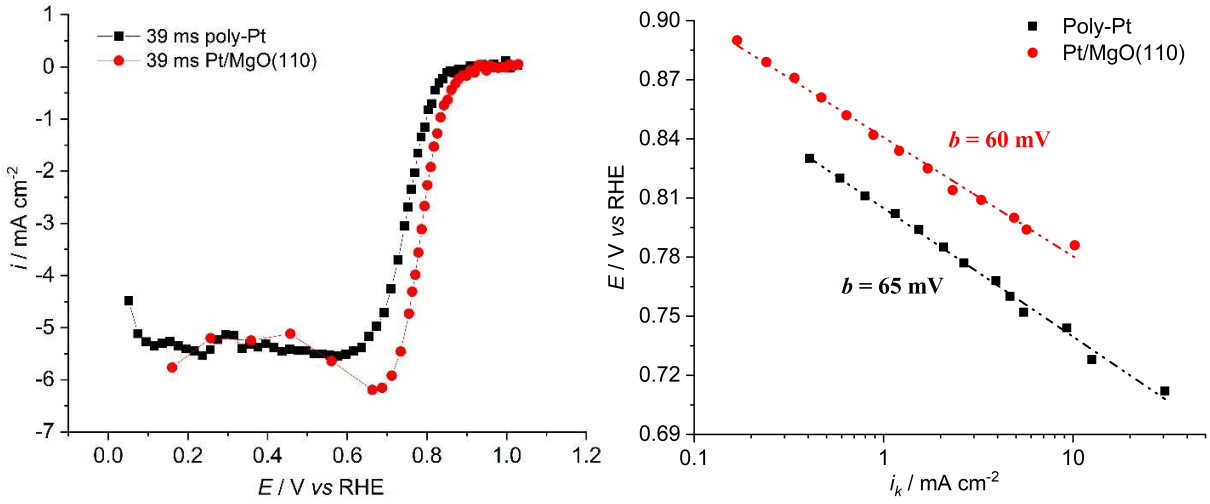

637

638 **Figure 6**

639

640

641

642